Design of an Efficient, Low Voltage, Third Harmonic, Large-Orbit Gyrotron Amplifier with a Vane-Resonator Output Cavity

Wes Lawson, *Member, IEEE*, W. W. Destler, Anna Fernandez, *Student Member, IEEE*, Arnold Liu, J. Rodgers, and Jonathan Weinstein

Abstract—**We present the design of a 100 kW, J-band, third harmonic large-orbit gyrotron amplifier which utilizes the interaction between a 45 kV, 4 A beam and a vane resonator output cavity operating in the "π"-mode. An efficiency of 55% is predicted with a large signal gain near 20 dB by a single particle code which takes into account nonideal effects associated with finite beam thickness and finite magnetic field transition widths. High efficiency is achieved by velocity modulation of an axially-streaming annular beam via a short TM_{310} drive cavity. Ballistically created axial bunches are converted into azimuthal bunches when the beam encounters a nonadiabatic, balanced magnetic field reversal at the end of a 30 cm drift region. The design of this tube is presented and its performance is completely characterized before the prospects for the operation of this low voltage configuration at other harmonics are explored.**

I. Introduction

MICROWAVE generation at high harmonics of the cyclotron frequency from large-orbit gyrotrons has undergone considerable theoretical and experimental scrutiny in the past two decades at a number of institutions [1]–[16]. Because of the reduced magnetic field requirements, these devices potentially have a considerable advantage over conventional first harmonic gyrotrons [17]–[19] in a number of applications that require compact, lightweight tubes. The chief disadvantage of high harmonic operation is the reduction in efficiency that usually accompanies any increase in harmonic number. One possible way to compensate for this weakness is to use energy recovery techniques to restore the net efficiency to a level comparable to the first harmonic devices [13], [20], [21]. Unfortunately, this approach adds to the complexity of the power supply and microwave output system. Also, there is typically a large capital cost associated with the collector hardware (insulators, electrodes, magnets, etc.). Furthermore, this approach does nothing to reduce cathode loading requirements or space-charge effects in the gun and beam transport system.

An alternate approach to enhanced efficiency involves prebunching the beam to achieve a nonuniform phase-space distribution prior to the entrance of the output cavity. Several such efficiency enhancement techniques have been attempted in linear devices [22]–[24], and all of them may be applicable to those large-orbit devices which introduce perpendicular energy into the beam via a nonadiabatic, magnetic field reversal. One of these techniques utilizes a modified version of the klystron's ballistic bunching process to generate the required velocity distribution. A device based on this technique, which we call the axially-modulated, cusp-injected, large-orbit gyrotron, has been explored in an earlier paper for a system with a 100 kV, 25 A beam [25].

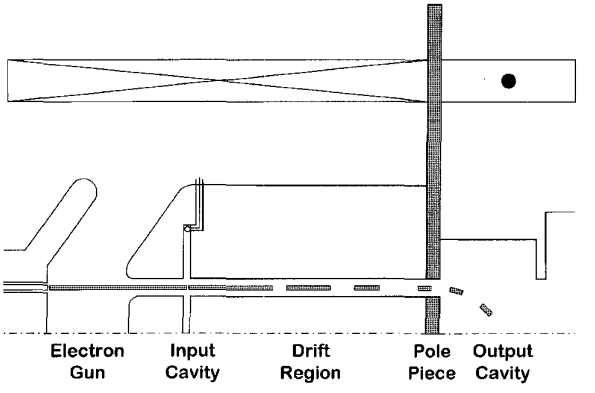

Fig. 1. A schematic of the axially-modulated, cusp-injected, large-orbit gyrotron.

A schematic of this device is shown in Fig. 1. The axial bunches are created ballistically after the beam passes through an input cavity which is driven with a TM_{m10} circularly-polarized mode. For $m > 0$, the proper mode is generated by utilizing two coupling ports on the outer wall which are spaced appropriately and are out of (time) phase by 90°. The axial bunches are converted into azimuthal bunches when the beam encounters the nonadiabatic magnetic transition (cusp). If the drive frequency is at the mth harmonic of the cyclotron frequency, the net effect is that the beam will form m spokes that will rotate at the cyclotron frequency. If an output cavity that operates in a TE_{mnp} mode is placed immediately after the cusp, efficient energy extraction can occur. For example, the previous design study demonstrated that an efficiency of 40% was achievable in X-Band at the fourth harmonic via an interaction with a right-circular TE_{411} cavity.

While the result quoted in the previous paragraph appears promising, there are some practical limits to the applicable range of parameters for this device. Of particular concern is the quality factor required to produce the optimal field strength in

Manuscript received November 3, 1995; revised February 14, 1996. The review of this paper was arranged by Editor J. A. Dayton, Jr. This work was supported by the Department of Defense Tri-Services Program for Vacuum Electronics.

The authors are with the Department of Electrical Engineering and the Institute for Plasma Research, University of Maryland, College Park, MD 20742 USA.

Publisher Item Identifier S 0018-9383(96)04033-6.

a low voltage, low current device operating at a high harmonic number. For example, the radius of the maximum electric field in a cavity, relative to the wall radius, increases with increasing harmonic number. Thus, the higher the harmonic number the further out the beam should be. However, the beam radius of the large-orbit configuration is equal to the Larmor radius, which, for a particular cyclotron frequency, is proportional to the perpendicular velocity. Thus, the beam radius in low voltage systems decreases fairly rapidly with decreasing beam energy. These two seemingly incompatible requirements often combine to yield an unrealistic requirement on the output cavity quality factor.

There are at least two ways to overcome this difficulty and design efficient, low voltage, harmonic devices. One way is to use a pre-bunched, small-orbit beam. Axial modulation is a viable technique for this approach because a nonreversal, nonadiabatic magnetic transition can be use to generate the small orbit beam. The guiding center radius can be adjusted to place the beam at a location where the electric field is relatively strong. This approach has been investigated previously via the design of a second harmonic small-orbit system [26]. In this design, a 35 kV, 4 A beam was pre-bunched by a short TM_{020} cavity and interacted with a 10 cm long TE_{011} output cavity to theoretically produce over 70 kW of power in X-Band. The simulated efficiency and large-signal gain were approximately 53% and 20 dB, respectively, when the beam thickness and finite magnetic transition width were taken into consideration. At approximately 1800, the required output cavity quality factor was well below the resistive Q of 28 600 and the cavity was stable to all spurious modes. However, the simulations indicated that the quality factor of a comparable third harmonic system would be too large.

The second approach is to use a vane-resonator to couple various azimuthal modes together. The resultant cavity modes can support the necessary azimuthal field variation with a much lower cutoff frequency. Thus, the wall radius can be reduced considerably as compared to the smooth wall case and the interaction impedance can be significantly increased. This is the approach that we will investigate in this paper. In the next section we will discuss the basic amplifier configuration and describe the computer codes used in the analysis. In Section III, we will present the results of a third harmonic example which utilizes a 45 kV, 4 A beam to efficiently generate 100 kW of power at 5.5 GHz. These parameters were selected to facilitate a future proof of-principle experiment in our laboratory. In addition to characterizing tube stability and large-signal characteristics, we will also discuss the sensitivity of the device to parameter variations. The results of this study and prospects for high harmonic operation are summarized in the final section.

II. Device Operation and Modeling

A detailed description of the operation of this device was given in [25]. In this section we briefly note the key aspects of the design and simulation processes and detail only the novel aspects of this work, which involve the use of a vane resonator (VR) output cavity.

In order to maximize the circuit gain, the beam must be placed near the maximum of the axial electric field in the input cavity, which is increasingly close to the wall radius with increasing harmonic number. The wall radius in a TM_{m10} cavity is proportional to the drive signal's wavelength while the beam radius is tied to the magnetic field and the beam energy. This problem is easier to remedy than the analogous one with the output cavity: either the input cavity can be moved into the magnetic field's adiabatic compression region where the beam radius is larger (if one exists) or dielectrics can be inserted into the input cavity to decrease the wall radius. We have selected the latter approach for this design. Because the cavity is short and the beam is thin and streaming linearly in that region, there should be no problem with charge build-up. We model the cavity with a code that assumes three dielectric regions radially and calculates the quality factor assuming a good conducting (copper) wall and an ideal dielectric.

The required drift tube length d depends on the magnitude of the energy spread $(\Delta E/E_0)$ imparted to the beam

$$d = \beta_0 \lambda / (2\Delta E/E_0) \tag{1}$$

where β_0 is the streaming velocity (normalized to the speed of light) and λ is the EM wavelength (of the input cavity signal). The magnetic transition at the end of the drift region is shortened by a thin iron pole piece. Long solenoids on either side of the pole piece generate approximately constant axial magnetic fields in each region (B_c on the input side and B_0 on the output side). The axial magnetic field is modeled by a piece-wise linear function and the radial field is given by Maxwell's equations. The spread in beam energy translates into additional velocity spread after the magnetic transition. When the effects of the input cavity's magnetic fields are neglected, the induced spread can be approximated by [25]

$$\begin{aligned} \frac{\Delta v_z}{v_{z_0}} &= \frac{1}{2}\left[1 + \alpha^2 + \alpha^2\left(\gamma_0^2 - 1\right)\right]\frac{\Delta E}{E_0} \\ \frac{\Delta v_\perp}{v_{\perp_0}} &= -\frac{1}{2}\left(\gamma_0^2 - 1\right)\frac{\Delta E}{E_0}. \end{aligned} \tag{2}$$

In (2), γ_0 is the relativistic mass factor.

A single particle code is used to simulate the beam's motion through the input cavity, the drift region, and the nonadiabatic magnetic transition. Given the beam parameters, electrons are initially "launched" over a range of axial positions, times, and angles that represent the entirety of phase space (after taking into account any symmetries in the system). The initial velocities of the particles are assumed to be purely axial. A minimum of 100 particles are used to model the beam when zero radial beam thickness is assumed and more than 300 particles are used to model finite thickness beams. After a Runge-Kutta start-up, a predictor-corrector integration scheme is used to solve the equations of motion. Convergence is checked by varying the time step and the number of particles and by verifying conservation of energy and canonical angular momentum for each particle. This "buncher" code produces the phase space distributions of the electrons at the end of the transition region, calculates the key beam statistics (e.g., the average velocity ratio and guiding center radius and the

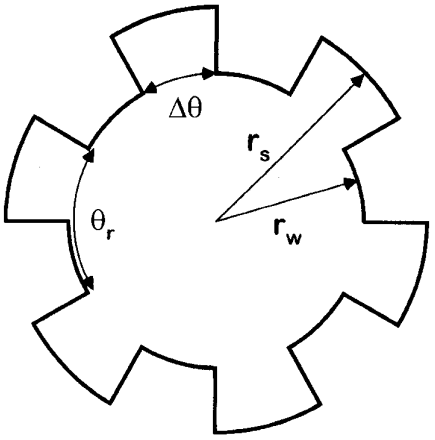

Fig. 2. Cross-sectional view of the vane resonator structure.

spreads in $v_\perp$, v_z, and energy), and indicates the effectiveness of the bunching process.

A cross-section of the output cavity is displayed in Fig. 2. The wall radius is denoted r_w and the slot depth is d_s so that the slot radius is $r_s = r_w + d_s$. We assume that there are n_s slots, so that the angular span of one period is $\theta_r = 2\pi/n_s$. The angular opening of each slot is $\Delta\theta$. To solve for the dispersion relation and subsequently the cutoff wavenumbers for the VR structure, we make the usual approximation of a constant electric field across the slot opening and match the magnetic field there only on average [13]. If we let the phase advance between adjacent slots be

$$\varphi_a = 2\pi l_0/n_s \tag{3}$$

where l_0 is an integer in the range $0 \le l_0 \le n_s$, then the dispersion relation is given by

$$\frac{J_0(x_w)Y_0'(x_s) - Y_0(x_w)J_0'(x_s)}{J_0'(x_w)Y_0'(x_s) - Y_0'(x_w)J_0'(x_s)} = \left(\frac{\Delta\theta}{\theta_r}\right)\sum_{q=-\infty}^{+\infty}\frac{J_{l_0+qn}(x_w)}{J'_{l_0+qn}(x_w)}\left\{\frac{\sin[(l_0+qn)\Delta\theta/2]}{(l_0+qn)\Delta\theta/2}\right\}^2. \tag{4}$$

Here $x_w = r_w\xi$ and $x_s = r_s\xi$, for $\xi = \sqrt{(\omega/c)^2 - k_z^2}$, and where ω is the angular frequency, c is the speed of light, and k_z is the axial wavenumber. $J_n(x)$ and $Y_n(x)$ are Bessel functions of the first and second kind, respectively.

A simple code is used to find the cutoff frequency of a VR structure from (4), given the dimensions listed above and a particular value of l_0. The usual two operating modes are the "π"-mode ($l_0 = n_s/2$) and the "2π"-mode ($l_0 = 0$). We will only consider the "π"-mode in this paper because it has in general a lower start-oscillation threshold than the other mode. The EM fields are generated by specifying an axial length for the cavity and assuming that the axial variation is sinusoidal (the closed cavity approximation). The resistive quality factor is calculated by assuming a good conductor (copper) wall, evaluating the magnetic field at all surfaces, and integrating the wall losses either analytically or numerically. The actual resistive Q will presumably be somewhat larger, since the endwalls will be partially removed.

A second single particle code takes the results from the "buncher" code and uses the same numerical techniques to calculate the extraction efficiency of the EM wave in the output cavity under steady-state conditions. The "efficiency" code also takes the results from the output cavity code to generate the electromagnetic fields. The applied dc magnetic field in the output cavity is assumed to vary linearly. This "efficiency" code is iterated, while varying the cavity and magnetic field parameters, until an optimal design is achieved. During each run, the amplitude and phase of the wave are adjusted until maximum efficiency is obtained. In addition to the efficiency, the code reports the required diffractive Q. By decreasing the field amplitude in the output cavity toward zero, this code is used to calculate the start currents for the various modes in tapered magnetic fields. The code has been benchmarked successfully against the start-oscillation results in [8] by using an unbunched beam.

III. Simulation Results for a Third Harmonic Design

The parameters for a third harmonic large-orbit design are given in Table I. The system is designed to produce microwaves at 5.5 GHz via the interaction between a 45 kV, 4 A beam and the microwave circuit. Given the beam energy and the expected magnetic field level, the beam radius of 1.125 cm is required to provide a velocity ratio near 2.2. This beam can be generated with a thin annular cathode and a modest magnetic compression. For example, a compression of about seven would result in a cathode loading of slightly above 1 A/cm^2, an average emitter radius of 3 cm, and a cathode thickness of 2 mm. The radial thickness indicated corresponds to an ideal post-cusp velocity spread from canonical angular momentum considerations of about $\Delta v_\perp = 1.9\%$. The dc space charge depression in the entire circuit is negligible.

The drive cavity is a dielectric-loaded, right-circular TM_{310} cavity with the dimensions indicated in Table I. The cavity width is selected to give a beam coupling factor [27] of about 0.98. A dielectric with a relative permittivity of about 13 is assumed to be placed above and below the beam location, leaving a clearance of at least 1 mm. The cavity radius is adjusted to achieve the desired operating frequency. With these parameters, the axial electric field shown in Fig. 3 is realized. Thus, the beam is located in a region where the electric field is nearly constant and optimal. The azimuthal magnetic field is also indicated in the figure. This field is quite small near the beam radius and has little effect on particle motion. The radial magnetic field is similar in profile to the electric field and is not shown. There are a number of good dielectrics with relative permittivities near 10 and we expect that a real device would use one of these and would also possibly place the cavity near the end of the magnetic compression region to maximize the gain.

The dc magnetic field profile throughout the circuit is determined during the efficiency optimization procedure. The axial magnetic field at the entrance to the output cavity is such that three times the cyclotron frequency is about 14% lower than the drive frequency. The 13% uptaper leaves the drive frequency nearly equal to thrice the cyclotron frequency at

TABLE I
THIRD HARMONIC AMPLIFIER SYSTEM PARAMETERS

Beam Parameters	
Voltage (kV)	45
Current (A)	4
Average radius (cm)	1.125
Beam thickness (mm)	0.75
Streaming velocity β_0	0.394
Velocity ratio ($v_\perp/v_z$)	2.200
Input Cavity	
Drive frequency (GHz)	5.5
Operating mode	TM_{310}
Resistive Quality factor (Q)	2170
Radius (cm)	1.701
Length (cm)	0.225
Magnetic Field Parameters	
Buncher magnetic field (G)	-567
Output magnetic field (G)	613
Cyclotron frequency (GHz)	1.577
Cusp width (cm)	0.375
Cavity - cusp spacing (cm)	30
Output field taper	13%
Output cavity	
Output frequency (GHz)	5.5
Operating mode	π-mode
Diffractive Q	1240
Resistive Q	13,430
Length (cm)	15.000
Radius (cm)	1.763
Slot depth (cm)	0.747
Slot width (%)	50
Number of vanes	6

the output cavity end. The magnetic transition is not perfectly balanced; the field strength in the drift region is about 8% lower than the initial field after the transition. The distance between the input cavity and cusp transition is optimized with the numerical codes, but the initial length is chosen from (1) so that maximal bunching could be achieved with an energy spread under 4%. The transition width should readily achievable with the aid of one or more iron pole pieces.

The length of the output cavity is varied to maximize efficiency while keeping the required Q less than 10% of the resistive Q of a copper cavity. This restriction allows for extraction of about 90% of the microwave power. The chosen length is such that unperturbed particles undergo approximately 4 1/2 revolutions inside the cavity. The cavity radius is selected to minimize beam interception and the slot depth is adjusted to produce the required resonant frequency. Six vanes are required for "π"-mode operation. The slot opening is fixed at 50% of the angular period. The azimuthal electric field and axial magnetic field radial profiles are plotted in Fig. 4 at a fixed azimuthal location which corresponds to the center of a vane. They are, of course, out of time phase by 90°. The discontinuity in the curves at r_w results from the truncation of the infinite series in (4). The azimuthal electric

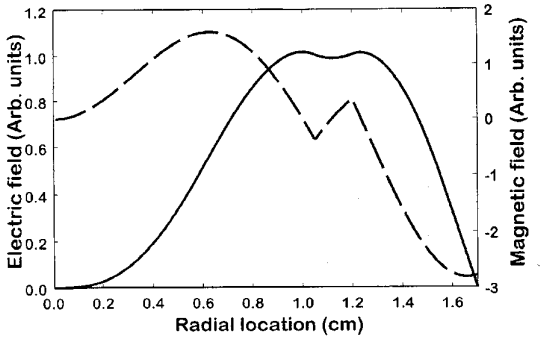

Fig. 3. Input cavity field radial profiles: Axial electric field (solid line) and azimuthal magnetic field (dashed line).

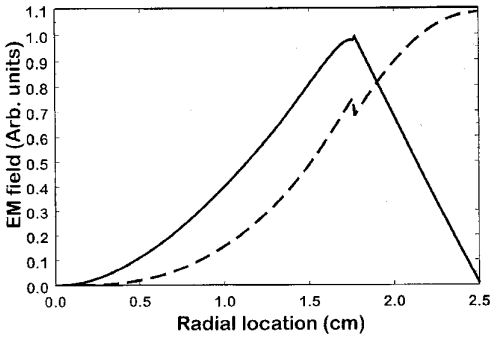

Fig. 4. Output cavity field radial profiles: azimuthal electric field (solid line) and axial magnetic field (dashed line). The azimuthal angle is fixed at the center of a vane opening.

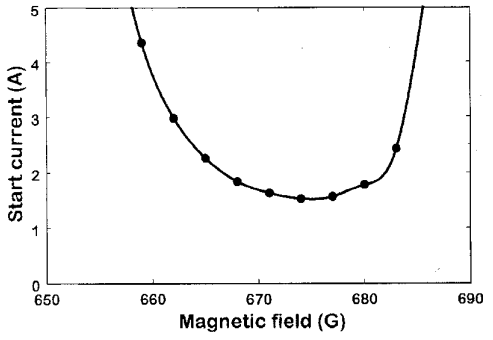

Fig. 5. The dependence of the start-oscillation current on magnetic field for the "π"-mode.

field at the initial average beam radius is nearly half of the peak field.

The beam current required to achieve self-oscillation in the "π"-mode of the output cavity is shown in Fig. 5 as a function of (uniform) magnetic field. It is assumed that no drive power is applied to the input cavity. The resonant frequencies of the various azimuthal modes are given in Table II. The "π"-mode is the only unstable mode in the magnetic field range from 600 to 700 G. However, even the "π"-mode is stable for the optimal tapered magnetic field profile at the design current of 4 A. The optimal zero-drive efficiency is found to be 27% at a starting magnetic field of 662 G and a weak uptaper.

TABLE II
RESONANT FREQUENCIES OF THE VR STRUCTURE

l_o	Resonant frequency (GHz)
0	7.231
1	3.686
2	5.055
3	5.500

TABLE III
THIRD HARMONIC AMPLIFIER PERFORMANCE

Input cavity results	
Input drive power (kW)	1.16
E_z at beam (kV/cm)	11.3
Drift region results	
Total Δv_z (%)	9.07
Total $\Delta v_\perp$ (%)	2.50
Bunching effectiveness (%)	37.79
Energy spread Δ E (%)	3.88
Output cavity results	
Power (kW)	99.7
Efficiency (%)	55.4
Gain (dB)	19.3
E_ϕ at beam (kV/cm)	21.3

The simulated results for the parameters in Table I near the optimal drive power are summarized in Table III. The nominal electric field at the average beam location is about 11 kV/cm in the input cavity and almost double that in the output cavity. The total axial velocity spread includes a contribution of about 1.9% from energy spread, which is substantially below the estimate given in (2) because of ac magnetic field effects. The contribution to the perpendicular velocity spread from the energy spread is about 1.7%. The bunching effectiveness is quantified by computing the RMS angular distribution of particles at the entrance to the output cavity, relative to the phase of the EM wave. This value is scaled and subtracted from 100% to yield a value of 0% for a uniform beam and a value of 100% for a perfectly bunched beam. The nominal saturated gain is just above 19 dB. The simulated efficiency of 55% is more than twice the maximum unbunched efficiency and is comparable to or better than the optimal theoretical efficiencies of most first harmonic gyrotrons. With a 180 kW beam, about 100 kW of microwave power should be produced.

The axial evolution of electron bunching in the device at the optimal point is illustrated in Fig. 6, where the r-z projection of the trajectories of representative particles are plotted. The input cavity entrance is at $z = 0$. The scalloping of the beam in the drift region is due to the Lorentz force brought about by the radial magnetic field in the input cavity. Since the guiding center radius of the beam is nearly zero, a particle's radial location is a good indication of its energy. The interaction between the wave and the beam is quite strong, with many particles gaining energy in the first half of the cavity only to lose it in the second half. Clearly the cavity radius is just large enough to avoid beam scrape-off. A larger radius could be used, but the required quality factor would increase.

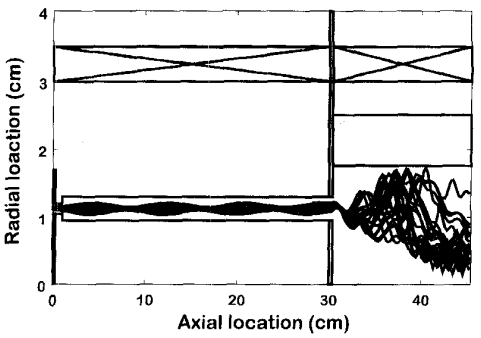

Fig. 6. Axial evolution of the radial location of representative particles for the optimal efficiency parameters.

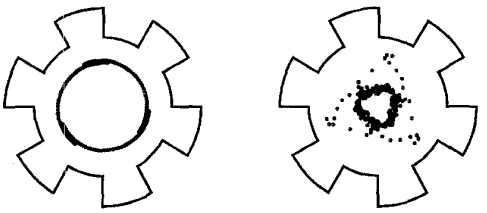

Fig. 7. The cross-sectional distribution of representative particles for the optimal efficiency parameters at (a) the entrance of the output cavity and (b) the exit of the output cavity.

Fig. 7(a) shows the distribution of representative particles in the transverse plane (for the same optimal parameters of Fig. 6) at the entrance to the output cavity. Though it is difficult to quantify the angular density distribution, three distinct particle bunches are clearly visible. The resultant phase distribution at the exit of the output cavity is shown in Fig. 7(b). The phase coherence of the beam is essentially destroyed and a large number of particles have given up the majority of their perpendicular energy. A much smaller number of particles have remained at about the same energy level or had their energy increase slightly.

The efficiency is plotted in Fig. 8 as a function of beam thickness. Also indicated in the figure is the axial velocity spread computed by the "buncher" code. The maximum efficiency of over 67% is obtained with a zero thickness beam. The efficiency drops steadily to about 55% at the nominal design thickness and begins to fall off more rapidly after that point. The bunching effectiveness (not plotted) is essentially independent of beam thickness. The required quality factor varies slowly from 1 070 at zero thickness to 1 240 at the 0.75 mm point and then jumps to 1 520 at the final point. The increase in velocity spread (from canonical angular momentum conservation) is believed to be the main cause for the decrease in efficiency. Beam scrape-off is probably also a contributing factor to the efficiency degradation, particularly at the final thickness point. If a shielded electron source, such as the Advanced Center-Post gun [28], were used instead of an immersed emitter, efficiencies for a finite thickness beam could approach 67%. In the remainder of this section we present mainly the characteristics of the zero-thickness (or shielded)

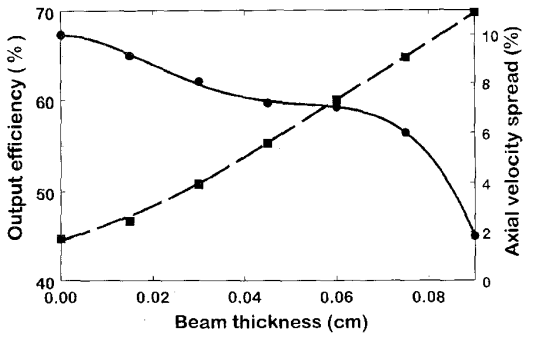

Fig. 8. The dependence of output efficiency (solid line) and total axial velocity spread (dashed line) on beam thickness.

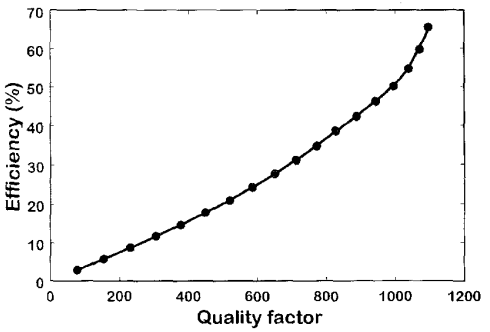

Fig. 10. The dependence of output efficiency on output cavity Q for the zero-thickness beam.

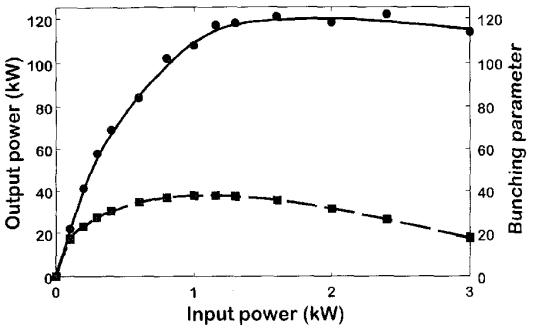

Fig. 9. The drive curve (solid line) for the zero-thickness beam when the output cavity Q is ~1 100. The dashed line indicates the bunching efficiency.

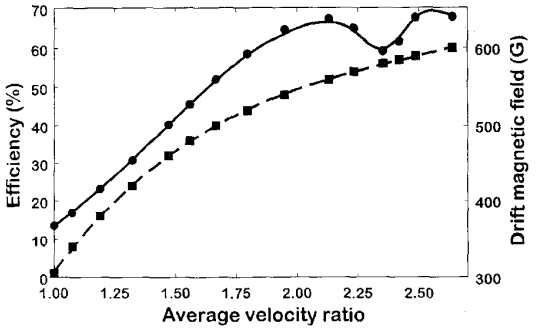

Fig. 11. The dependence of output efficiency on average velocity ratio (solid line). The required drift tube magnetic field is indicated by the dashed line.

beam; the characteristics of the 0.75 mm beam are found to be similar, with a reduction in efficiency of about 10% near the optimal power points.

The drive curve near the optimal system parameters (but with a zero thickness beam) is shown in Fig. 9. The relative bunching effectiveness is given in the figure by the dashed line. The curve is generated assuming a constant quality factor in the output cavity of about 1 100. The device is zero-drive stable and enjoys a fairly broad saturation region. The induced energy spread in the beam is about 6.2% at the maximum drive power of 3 kW.

The dependence of efficiency on output cavity Q is displayed in Fig. 10. All other parameters are held fixed at the optimal system configuration values. The output efficiency rises steadily from zero to about 45% as the quality factor is increased to 875. After that point, the efficiency increases more rapidly with Q until it reaches its maximum value of ~1 100. Electric fields that are indicative of quality factors above 1 150 result in beam scrape-off and consequently are not plotted. Undoubtedly, scrape-off could be avoided and comparable efficiencies achieved if we were to adjust some of the other parameters (e.g., magnetic field taper).

The dependence of output efficiency on the thin beam's average velocity ratio is given in Fig. 11. This ratio is modified solely by varying the magnetic field in the drift region; the required field at each point is indicated in the figure by the dashed line. The phase and amplitude of the output cavity's electric field are optimized at each point. This implies that the quality factor is adjusted to maximize output power. All other parameters, however, are held at their nominal values. The first maximum in efficiency is 67%, occurs near the nominal velocity ratio of 2.2, and drops off fairly rapidly with decreasing velocity ratio, going to a level of about 13% at a velocity ratio near one. The maximum quality factor of 1 850 is required at the minimum efficiency point. There is a dip in the efficiency near a velocity ratio 2.35 before it returns to the 67% level at a velocity ratio of 2.5. A buncher field of 610 Gauss yields a velocity ratio above 2.8 and results in particle reflections in the output cavity's tapered magnetic field.

IV. Discussion

In this paper we have demonstrated, via a concrete design, the feasibility of the low voltage, high efficiency, pre-bunched, gyrotron concept at the third harmonic. The principle extension of this work beyond our previous study [25] involves the introduction of a vane-resonator output cavity. This configuration allows a reduction in the transverse dimensions of the cavity for a given frequency and azimuthal mode number and results in vastly improved beam coupling to low energy, axis-encircling beams. With this approach, we are able to produce simulated efficiencies of 67% with a shielded beam and 55% with an immersed beam (which had an axial velocity spread of about 9%). With a beam voltage of 45 kV and a current of 4 A, the resultant power is 100 kW. The design is most sensitive to the required output cavity quality factor, which at

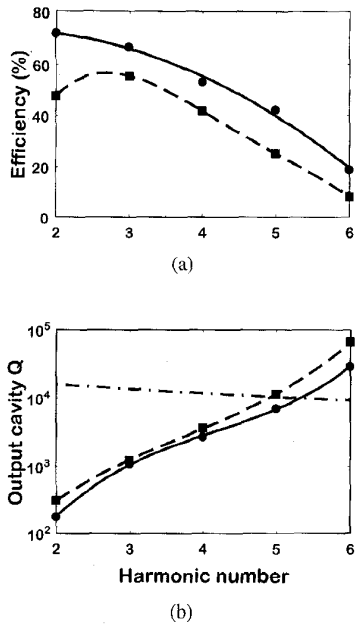

Fig. 12. (a) The efficiency as a function of harmonic number for a zero-thickness beam (solid line) and a 0.75 mm thick beam (dashed line). The output cavity length is fixed at 15 cm and the magnetic field taper is fixed at 13%, but the drive frequency is proportional to the harmonic number. The remaining design parameters are adjusted to be compatible with the drive frequency. (b) The required quality factor for the zero-thickness beam (solid line) and the finite thickness beam (dashed line).

the optimal point is acceptable at less than 10% of the output cavity's resistive Q.

We have also taken a preliminary look at efficiency enhancement in higher harmonic systems with comparable beam voltages. In Fig. 12(a), we plot the simulated efficiency of the large-orbit device as a function of harmonic number. The solid line indicates the simulated efficiency achievable for a zero-thickness beam and the dashed line gives the 0.75 mm beam result. The third harmonic point corresponds to the system described in the previous section. For the other harmonic results, the magnetic field and beam parameters are fixed at the values given in Table I. However, the cavity-cusp spacing, and the cavities' harmonic number, radial dimensions, and number of (output) vanes are adjusted to the appropriate values. Furthermore, the output cavity quality factor is adjusted to optimize efficiency. With the exception of the second harmonic result, the finite beam thickness results in an efficiency decrease of about 10–12%.

In Fig. 12(b) we plot the required output quality factors for the thin (solid line) and thick (dashed line) beams. Operation above the fourth harmonic is not practical because the required Q is comparable to or exceeds the resistive Q of a copper cavity (given by the dot-dashed line in the figure). These results for the higher harmonics can undoubtedly be improved upon by a more complete optimization (e.g., adjustment of the output cavity length), but the basic trend would still persist. Thus, operation at harmonics significantly above the fourth will require an increase in beam voltage and/or power.

In the near future, we will attempt a proof-of-principle experiment based on this concept. We are in the process of building a test bed which is energized by a 50 kV, 20 A, 5 μs pulse-line modulator. The frequency in this study is selected to be compatible with sources and magnetic field coils which are readily available to us. We are currently designing an electron gun that is compatible with the beam parameters of this design.

REFERENCES

[1] P. Sprangle, "Exicitation of electromagnetic waves from a rotating annular relativistic e-beam," *J. Appl. Phys.*, vol. 47, pp. 2935–2940, 1976.
[2] W. W. Destler, D. W. Hudgings, M. J. Rhee, S. Kawasaki, and V. L. Granatstein, "Experimental study of microwave generation and suppression in a nonneutral e-layer," *J. Appl. Phys.*, vol. 48, pp. 3291–3296, 1977.
[3] H. S. Uhm and R. C. Davidson, "Intense microwave generation by the negative-mass instability," *J. Appl. Phys.*, vol. 49, pp. 593–598, 1978.
[4] W. W. Destler, R. L. Weiler, and C. D. Striffler, "High-power microwave generation from a rotating E layer in a magnetron-type waveguide," *Appl. Phys. Lett.*, vol. 38, pp. 570–572, 1981.
[5] Y. Y. Lau and L. R. Barnett, "Theory of a low magnetic field gyrotron (gyromagnetron)," *Int. J. Infrared Millimeter Waves*, vol. 3, pp. 619–643, 1982.
[6] W. W. Destler, R. Kulkarni, C. D. Striffler, and R. L. Weiler, "Microwave generation from rotating electron beams in magnetron-type waveguides," *J. Appl. Phys.*, vol. 54, pp. 4152–4162, 1983.
[7] W. Namkung, "Observation of microwave generation from a cusptron device," *Phys. Fluids*, vol. 27, pp. 329–330, 1984.
[8] K. R. Chu and D. Dialetis, "Theory of harmonic gyrotron oscillator with slotted resonant structure," *Int. J. Infrared Millimeter Waves*, vol. 5, pp. 37–56, 1984.
[9] W. Lawson, W. W. Destler, and C. D. Striffler, "High-power microwave generation from a large-orbit gyrotron in vane and hole-and-slot conducting wall geometries," *IEEE Trans. Plasma Sci.*, vol. PS-13, pp. 444–453, 1985.
[10] W. Lawson and C. D. Striffler, "A general linear growth rate formula for large orbit, annular electon beams," *Phys. Fluids*, vol. 28, pp. 2868–2877, 1985.
[11] ——, "A linear growth rate fluid formulation for large orbit, annular electron layers with finite thickness," *Phys. Fluids*, vol. 29, pp. 1682–1694, 1986.
[12] E. Chojnacki, W. W. Destler, W. Lawson, and W. Namkung, "Studies of microwave radiation from a nonrelativistic rotating electron beam in a multiresonator magnetron cavity," *J. Appl. Phys.*, vol. 61, pp. 1268–1275, 1987.
[13] W. W. Destler, E. Chojnacki, R. F. Heoberling, W. Lawson, A. Singh, and C. D. Striffler, "High-power microwave generation from large-orbit devices," *IEEE Trans. Plasma Sci.*, vol. 16, pp. 71–89, 1988.
[14] W. W. Destler, K. Irwin, W. Lawson, J. Rodgers, Z. Segalov, E. P. Scannell, and S. T. Spang, "Intense-beam fundamental mode large-orbit gyrotron studies," *J. Appl. Phys.*, vol. 66, pp. 4089–4094, 1989.
[15] C. S. Kou, D. B. McDermott, N. C. Luhmann Jr., and K. R. Chu, "Prebunched high-harmonic gyrotron," *IEEE Trans. Plasma Sci.*, vol. 18, pp. 343–349, 1990.
[16] K. K. Tiong and S. P. Kuo, "Operation of a high harmonic cusptron oscillator," *Int. J. Electronics*, vol. 70, pp. 815–821, 1991.
[17] R. S. Symons and H. R. Jory, *Advances in Electronics and Electron Physics*, C. Marton, Ed. New York: Academic, 1981, vol. 55, chap. 1, p. 1.
[18] V. L. Granatstein, M. E. Read, and L. R. Barnett, *Infrared and Millimeter Waves*, K. Button, Ed. New York: Academic, vol. 5, chap. 5, p. 267, 1981.
[19] K. E. Kreischer, T. L. Grimm, W. C. Guss, A. W. Mobins, and R. J. Temkin, "Experimental study of a high-frequency megawatt gyrotron oscillator," *Phys. Fluids B*, vol. 2, pp. 640–646, 1990.
[20] A. Singh, W. Lawson, D. Goutos, W. R. Hix, C. D. Striffler, V. L. Granatstein, and W. W. Destler, "Beam conditioning for electron energy recovery systems in devices employing axis-encircling beams," *Int. J. Electron.*, vol. 65, pp. 351–368, 1988.
[21] M. E. Read, W. Lawson, A. J. Dudas, and A. Singh, "Depressed collectors for high power gyrotrons," *IEEE Trans. Electron Devices*, vol. 37, pp. 1579–1589, 1990.
[22] H. M. Bizek, P. M. McIntyre, D. Raparia, and C. A. Swenson, "Gigatron," *IEEE Trans. Plasma Sci.*, vol. 16, pp. 258–263, 1988.
[23] M. Yoshioka, "Lasertron: A pulsed rf source using a laser-triggered photocathode," *Jap. J. Appl. Phys.*, vol. 28, pp. 1079–1093, 1989.

[24] D. H. Preist and M. B. Shrader, "The klystrode—An unusual transmitting tube with potentials for UHF-TV," *Proc. IEEE*, vol. 70, pp. 1318–1325, 1982.
[25] W. Lawson and W. W. Destler, "The axially modulated, cusp-injected, large-orbit gyrotron amplifier," *IEEE Trans. Plasma Sci.*, vol. 22, pp. 895–901, 1994.
[26] W. Lawson, A. Grigoropolous, A. Liu, G. P. Saraph, J. Rodgers, and W. W. Destler, "Design of a high efficiency, low voltage, axially modulated, cusp-injected, second harmonic, X-band gyrotron amplifier," submitted to *IEEE Trans. Plasma Sci.*, Aug. 1995.
[27] R. E. Collin, *Foundations for Microwave Engineering*. New York: McGraw-Hill, 1966, p. 468.
[28] G. P. Scheitrum, T. Bemis, T. A. Hargreaves, and L. Higgins, "95 GHz harmonic gyroklystron," in *Proc. SPIE*, 1993, vol. 2104, pp. 523–524.

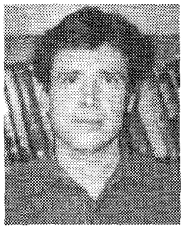

Wes Lawson (S'84–M'85) received the B.S. degree in mathematics (1980) and the B.S. (1980), M.S. (1981), and Ph.D. (1985) degrees in electrical engineering from the University of Maryland, College Park. His dissertation work involved theoretical and experimental studies of microwave generation in various large-orbit gyrotron configurations.

He worked in the Electronic Systems Branch of Harry Diamond Laboratories from 1978 to 1982. He has been with the University of Maryland's Laboratory for Plasma Research for the past 13 years and is currently an associate professor in the Department of Electrical Engineering. His principle interest lies in novel fast-wave microwave sources and his recent efforts have been directed toward high power fast-wave and hybrid amplifiers and associated high power microwave components.

W. W. Destler, photograph and biography not available at the time of publication.

Anna Fernandez (S'95) was born in Falls Church, VA in 1975. For the past year she has been working at the Institute for Plasma Research as an undergraduate research assistant while pursuing the B.S. degree in electrical engineering at the University of Maryland, College Park.

Arnold Liu was born in Columbia, MD, in 1976. For the past year he has been working at the Institute for Plasma Research as an undergraduate research assistant while pursuing the B.S. degree in electrical engineering at the University of Maryland, College Park.

J. Rodgers received the B.S. degree in electrical engineering from the University of Maryland, College Park, in 1987.

He served on active duty in the U.S. Navy from 1975 to 1981, and from 1981 to 1987, he served in the U.S. Navy Reserves as an electronics technician working on shipboard satellite, ultra-high frequency, and airborn communications systems, and on high-power microwave radar and tactical navigation. In 1981, he joined the Satellite Reliability Group at the Applied Physics Laboratory, Johns Hopkins University, Baltimore, MD, where he worked on qualifying new hardware for the GEOSAT, AMPTE, and Hopkins Ultra-Violet Telescope programs, while attending night school at the same university. In 1987, he joined the the Institute for Plasma Research, University of Maryland, College Park, as a Faculty Assistant. His efforts have concentrated on the study of the physics of charged particle beams with application to collective acceleration, beam transport, and the generation of intense, coherent radiation. The topics to which he has contributed include laser-controlled collective ion acceleration, ultra-high power microwave propagation in atmosphere, large orbit, and harmonic gyrotrons, free-electron lasers, microwave material processing, microwave-plasma interactions, and high-power, slow-wave microwave devices. He has coauthored over 25 papers in refereed journals covering these and other related topics.

Jonathan Weinstein was born in Washington, D.C. in 1972. He received the B.S. degree in electrical engineering from The Pennsylvania State University, University Park, in December, 1994. For the past year he has been working at the Institute for Plasma Research as an graduate research assistant while pursuing the M.S. degree in electrical engineering at the University of Maryland, College Park.